Supplementary Materials for

A 3D study on the amplification of regional haze and particle growth by local emissions

Wei Du[1,2,#], Lubna Dada[2,#], Jian Zhao[1,3], Xueshun Chen[1], Kaspar R. Daellenbach[2], Conghui Xie[1,3], Weigang Wang[4], Yao He[1,3], Jing Cai[2], Lei Yao[2], Yingjie Zhang[1], Qingqing Wang[1], Weiqi Xu[1], Yuying Wang[5], Guiqian Tang[1], Xueling Cheng[1], Tom V Kokkonen[2], Wei Zhou[1,3], Chao Yan[2], Biwu Chu[2], Qiaozhi Zha[2], Simo Hakala[2], Mona Kurppa[2], Leena Järvi[2,6], Yongchun Liu[7], Zhanqing Li[8], Maofa Ge[4], Pingqing Fu[1,3], Wei Nie[9], Federico Bianchi[2], Tuukka Petäjä[2,9], Pauli Paasonen[2], Zifa Wang[1,10], Douglas R. Worsnop[11], Veli-Matti Kerminen[2], Markku Kulmala[2,7,9,*], Yele Sun[1,3,10,*]

Affiliations:

[1] State Key Laboratory of Atmospheric Boundary Layer Physics and Atmospheric Chemistry, Institute of Atmospheric Physics, Chinese Academy of Sciences, Beijing 100029, China

[2] Institute for Atmospheric and Earth System Research/Physics, Faculty of Science, University of Helsinki, P.O. Box 64, Helsinki 00014, Finland

[3] College of Earth and Planetary Sciences, University of Chinese Academy of Sciences, Beijing 100049, China

[4] State Key Laboratory for Structural Chemistry of Unstable and Stable Species, Institute of Chemistry, Chinese Academy of Sciences, Beijing 100190, China

[5] School of Atmospheric physics, Nanjing University of Information Science and Technology, Nanjing 210044, China

[6] Helsinki Institute of Sustainability Science, University of Helsinki, Yliopistokatu 3, 00014, University of Helsinki, Finland

[7] Aerosol and Haze Laboratory, Beijing Advanced Innovation Center for Soft Matter Science and Engineering, Beijing University of Chemical Technology, Beijing 100029, China

[8] College of Global Change and Earth System Science, Beijing Normal University, Beijing 100875, China

[9] Joint International Research Laboratory of Atmospheric and Earth System Sciences, School of Atmospheric Sciences, Nanjing University, Nanjing 210023, China

[10] Center for Excellence in Regional Atmospheric Environment, Institute of Urban Environment, Chinese Academy of Sciences, Xiamen 361021, China

[11] Aerodyne Research, Inc., Billerica, MA 01821, USA

[#] These authors contributed equally to this paper.

[*] **Corresponding authors:**

Yele Sun: sunyele@mail.iap.ac.cn

Markku Kulmala: markku.kulmala@helsinki.fi

Supplementary Methods

Particle number size distributions

Two Scanning Mobility Particle Sizers (SMPS) were deployed to simultaneously measure the particle number size distributions at ground level and 260 m. At 260 m, the size-resolved particle number concentrations (15-685 nm, flow rate 0.3 L min^{-1}) were measured in situ by an SMPS based on a Condensation Particle Counter (CPC, TSI, 3775) and a long Differential Mobility Analyzer (DMA, TSI, 3081A) at a time resolution of 5 min. At ground level, an SMPS as part of an unattended multifunctional hygroscopicity tandem differential mobility analyzer (H-TDMA) developed by the Guangzhou Institute of Tropical and Marine Meteorology, China Meteorological Administration (ITMM, CMA) was used to measure particle number concentrations (10-400 nm, flow rate 1 L min^{-1}) from August 22th to October 1st, 2015. Similarly, a Condensation Particle Counter (CPC, TSI, 3772) equipped with long Differential Mobility Analyzer (DMA, TSI, 3081A) was used to measure size-resolved particle number concentrations (11-552 nm, flow rate 1 L min^{-1}) from November 21th to December 13th, 2016 and from June 1st to 26th, 2017. In front of the sampling system at both heights, silica gel diffusion dryers were applied to keep the sample flow with relative humidity less than 40%. Before the campaign in winter 2016 and after the campaign in summer 2017, the two SMPS were deployed for two days using the same sampling line for inter-comparisons. The results showed that size distributions of particle number concentrations showed excellent agreement (Supplementary Figure 19). According to previous comparisons of particle number size distributions between different SMPSs or differential mobility particle sizers, the measurement uncertainties between 20 and 200 nm can be ~ 10 %, and even larger for particles outside this range [1].

Aerosol particle composition

A high-resolution aerosol mass spectrometer (HR-AMS, Aerodyne Research Inc.) and an aerosol chemical speciation monitor (ACSM, Aerodyne Research Inc.) were used to measure non-refractory submicron aerosol (NR-PM_1) species, including organics, sulfate, nitrate, ammonium and chloride at ground level (~8 m) and 260 m, respectively [2]. The ambient air was drawn into the sampling room through a stainless-steel tube with the flow rate of 10 L min^{-1} (~ 0.085 L min^{-1} was sampled into the HR-AMS) at ground and 3 L min^{-1} (~ 0.1 L min^{-1} was sampled into the ACSM) at 260 m. $PM_{2.5}$ cyclones were supplied in front of the sampling lines for both HR-AMS and ACSM to remove coarse particles larger than 2.5 μm. Before sampling into HR-AMS and ACSM, aerosol particles were dried by diffusion silica gel dryers to avoid water vapor condensation which reduces the uncertainties in particle collection efficiency (CE) due to variable relative humidity.

The raw mass spectra of HR-AMS were analyzed using the Igor based packages PIKA v. 1.16H and SQUIRREL v. 1.57H. The ACSM data were analyzed using the standard data analysis software v. 1.5.3.0. We applied the default relative ionization efficiency (RIE) values to convert raw signals to mass concentrations, except that of ammonium which was calibrated from pure ammonium nitrate [3]. Collection efficiency (CE)= 0.5 was used after considering the effects of ammonium nitrate, relative humidity, and particle acidity [4]. Considering the different aerosol mass spectrometers might introduce additional uncertainties in comparisons between ground level and 260 m, we performed an inter-comparison study between HR-AMS and ACSM for two weeks. the HR-AMS and ACSM measured species tracked well (r^2 = 0.97-1.0) [5], and the regression slopes were applied to ACSM measurements to better compare with AMS measurements.

During the campaign of 2015, a two-wavelength aethalometer (AE22, Magee Scientific Corp.) and a seven-wavelength aethalometer (AE33, Magee Scientific Corp.) were deployed at ground level and at 260 m, respectively to measure black carbon (BC) concentrations. The measurements from the two different aethalometers agree well during the one-week inter-comparison at ground level (r^2=0.99) [2]. Compared with 2015, the two same types of AE33 were deployed at ground level and 260 m during years of 2016 and 2017.

Gaseous species

At ground level, a cavity-attenuated phase shift NO_2 monitor (CAPS NO_2, Aerodyne Research Inc.) was deployed to measure NO_2. Other gaseous species of CO, SO_2, O_3, and NO_x were measured by a suite of gas analyzers including CO analyzer (Thermo, 48*i*), SO_2 analyzer (Thermo, 43*i*), O_3 analyzer (Thermo, 49*i*), and nitrogen oxide analyzer (Thermo, 42i). At 260 m, gaseous species of CO, SO_2, O_3 were recorded from November 21 to December 13, 2016 and from June 1 to 26, 2017 using the same types of gas analyzers as those at ground level.

Meteorological parameters

The meteorological parameters, including wind speed (WS), wind direction (WD), relative humidity (RH), and temperature (*T*) were obtained from the BMT at 15 heights (8, 15, 32, 47, 63, 80, 102, 120, 140, 160, 180, 200, 240, 280, and 320 m).

The instrument used to observe the mixing layer height (MLH) was a single-lens ceilometer (CL51, Vaisala, Finland). This instrument utilizes pulsed diode laser lidar technology (910 nm waveband) to measure the attenuated backscatter coefficient profile. We cleaned CL51 lens with clear water every 3 days owing to the relatively high aerosol concentration in Beijing.

We determined the MLH as described in Tang et al.[6]. Because the particle concentration in the mixing layer and that in the free atmosphere are significantly different, the top of atmospheric mixing layer is the position at which a sudden change occurs in the attenuated backscatter coefficient profile. In our study, we used the Vaisala software product BL-VIEW to determine the MLH by selecting the location with the maximum negative gradient ($-d\beta/dx$) in the attenuated backscatter coefficient profile as the top of the mixing layer. To eliminate the influence of inherent noise and aerosol layers on the data, spatial and temporal averaging must be carried out before the gradient method is used to calculate the MLH. Time averaging is dependent on the current signal noise; the intervals vary from 14 to 52 min for the CL51. Height averaging intervals range from 80 m at ground level to 360 m at 1600 m height and beyond. Additional features of this algorithm, which is used in the Vaisala software product BL-VIEW, are cloud and precipitation filtering and outlier removal.

Particle Diameter and Densities

Two different diameters were used in parallel throughout this study including mobility diameter (D_m) for SMPS measurements and vacuum aerodynamic diameter (D_{va}) for AMS measurements. Assuming spherical particles, D_{va} approximately equals particle density (ρ_{comp}) times D_m, which is written as D_p in this study [7]. The particle density can be estimated with the measured submicron aerosol composition using Eq. (1) (35):

$$\rho_{comp} = \frac{[NO_3^-]+[SO_4^{2-}]+[NH_4^+]+[Cl^-]+[BC]+[Org]}{\frac{[NO_3^-]+[SO_4^{2-}]+[NH_4^+]}{1.75}+\frac{[Cl^-]}{1.52}+\frac{[BC]}{1.77}+\frac{[Org]}{1.2}} \quad (1)$$

where the densities are 1.75 g cm^{-3} for ammonium nitrate and ammonium sulfate, 1.52 g cm^{-3} for ammonium chloride, 1.2 g cm^{-3} for organic aerosols and 1.77 g cm^{-3} for BC.

Supplementary Figures

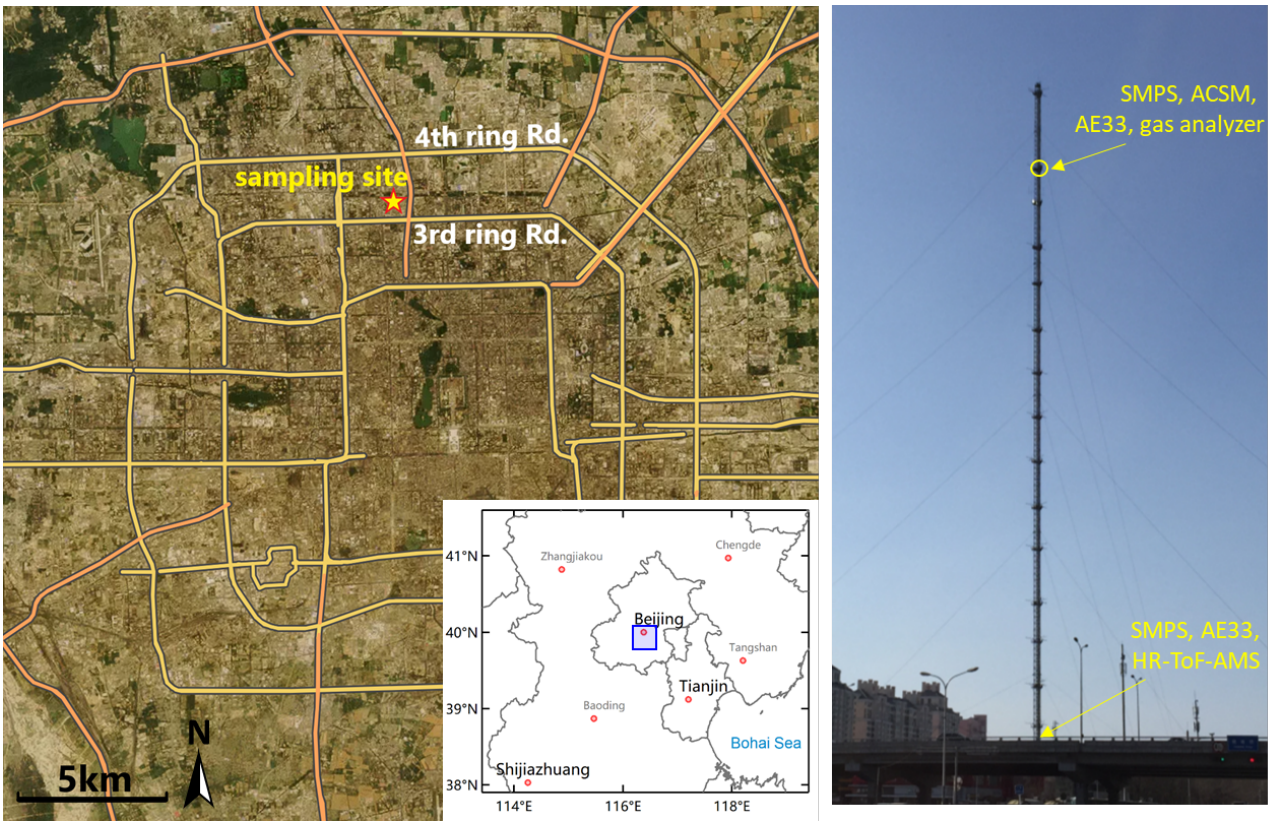

Supplementary Figure 1. Location of the sampling site and the Beijing 325 m meteorological tower. The measurements were conducted at ground level (SMPS, AE33, and HR-ToF-AMS), and 260 m (SMPS, ACSM, AE33, and gas analyzers).

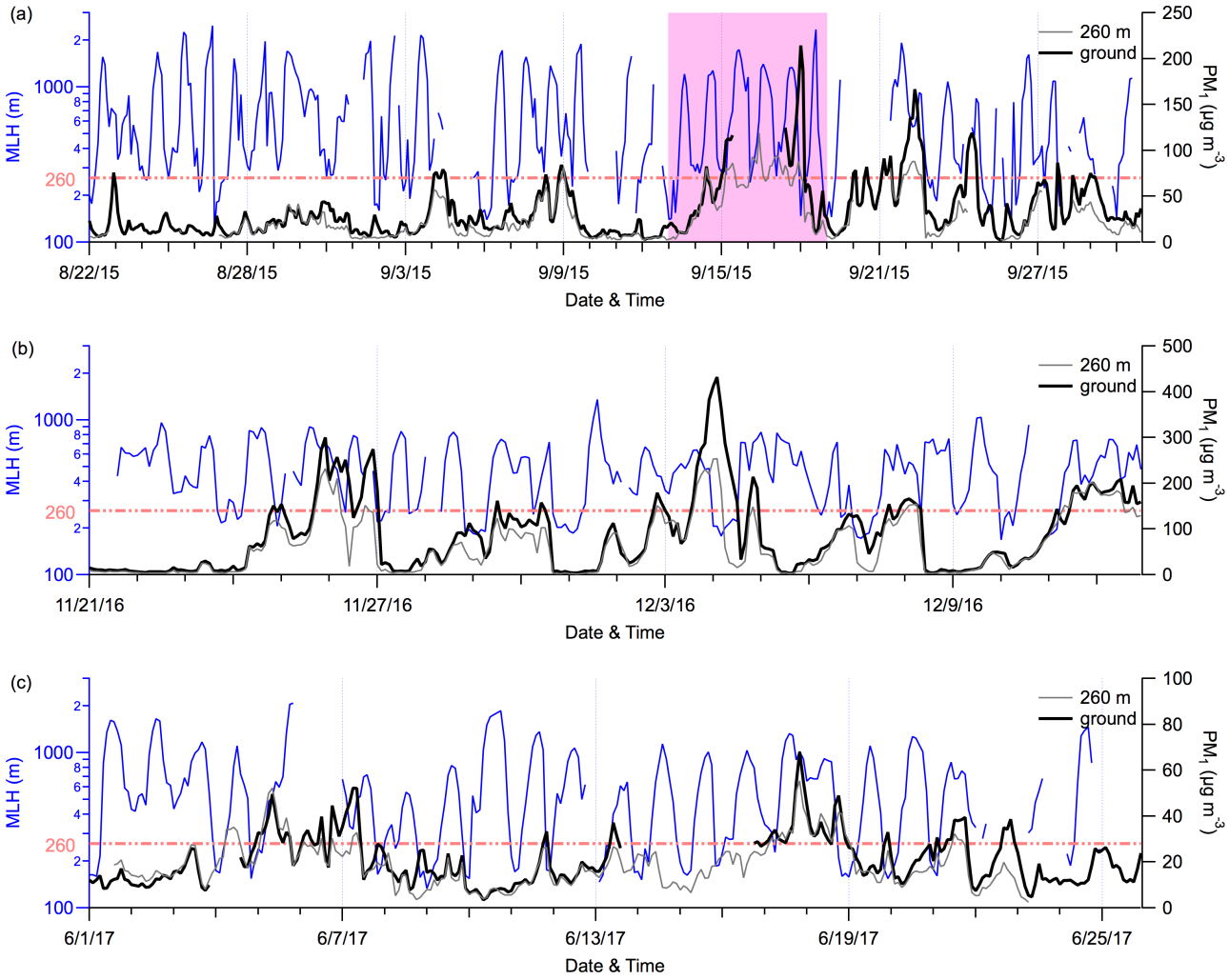

Supplementary Figure 2. The time series of mixing layer height (MLH) and mass concentration of submicron aerosols (PM_1) at 260 m and ground level (a) from August 22 to October 1, 2015, (b) from November 21 to December 13, 2016, (c) from June 1 to 26, 2017. The pink area shows the case from September 13 to 19, 2015.

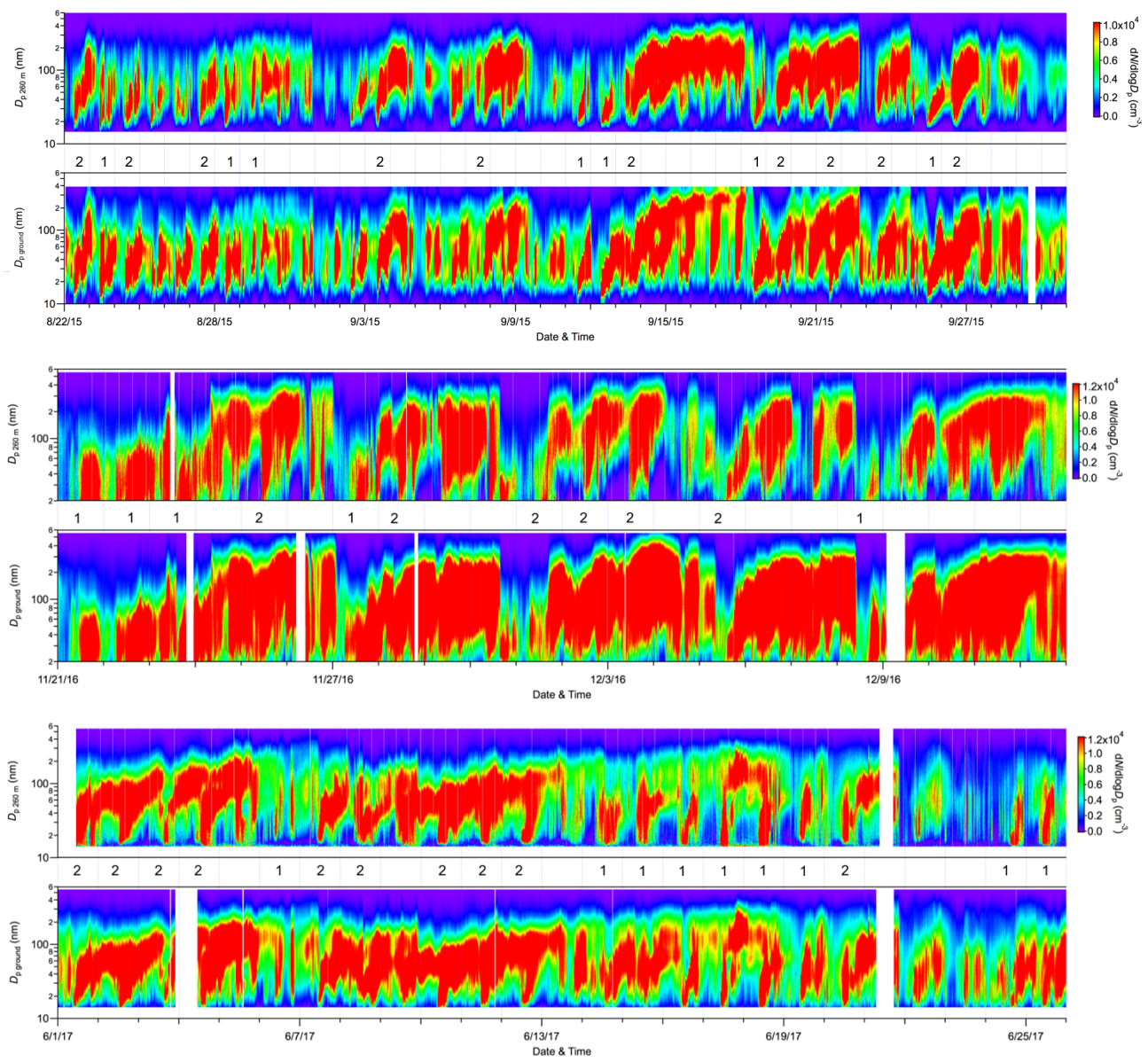

Supplementary Figure 3. The evolution of size-resolved particle number concentration at 260 m and ground level (a) from August 22 to October 1, 2015, (b) from November 21 to December 13, 2016, (c) from June 1 to 26, 2017. The number 1, 2 represent the NPF-1 and NPF-2, respectively.

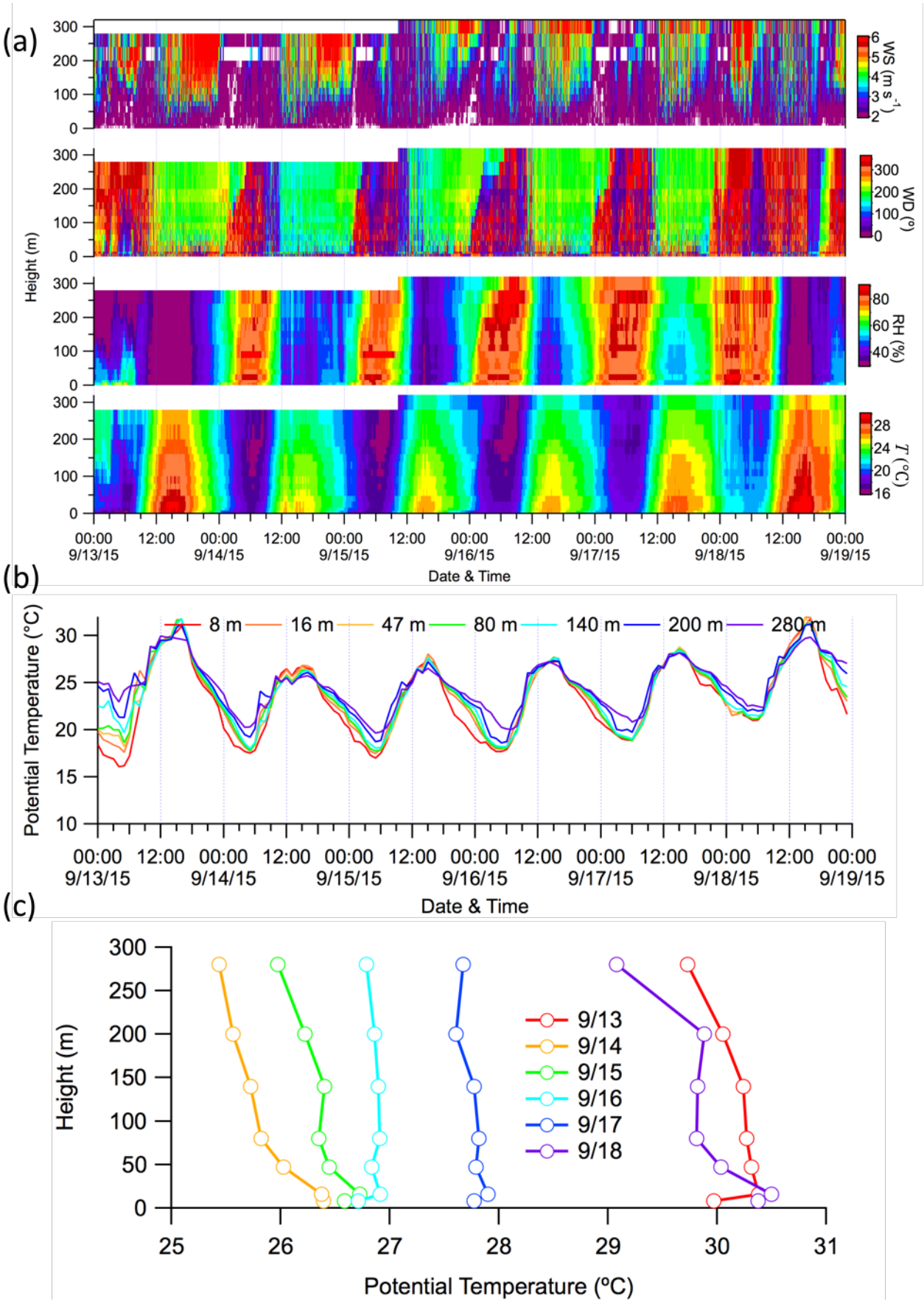

Supplementary Figure 4. (a) The variation of wind speed, wind direction, relative humidity, and temperature observed from the meteorological tower, (b) the evolution of calculated potential temperature at different heights

including 8 m, 16 m, 47 m, 80 m, 140 m, 200 m, 280 m, and (c) the average potential temperature profile in the afternoon (12:00 – 18:00) during the severe pollution period of September 13 – 19, 2015.

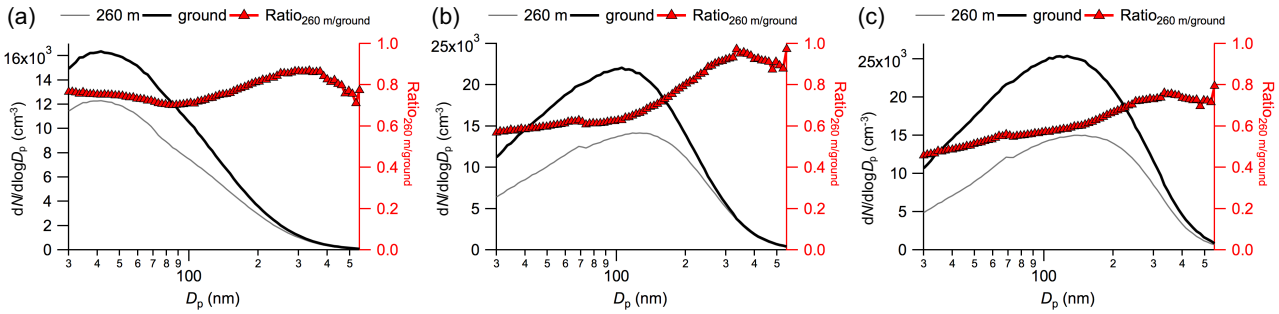

Supplementary Figure 5. Average particle number size distribution at 260 m and at ground level during the campaign in 2016 when (a) $PM_1 < 50$ μg m^{-3}, (b) $50 < PM_1 < 100$ μg m^{-3}, (c) $PM_1 > 100$ μg m^{-3}. The red triangle shows the ratios of size-resolved particle number concentration between the two heights.

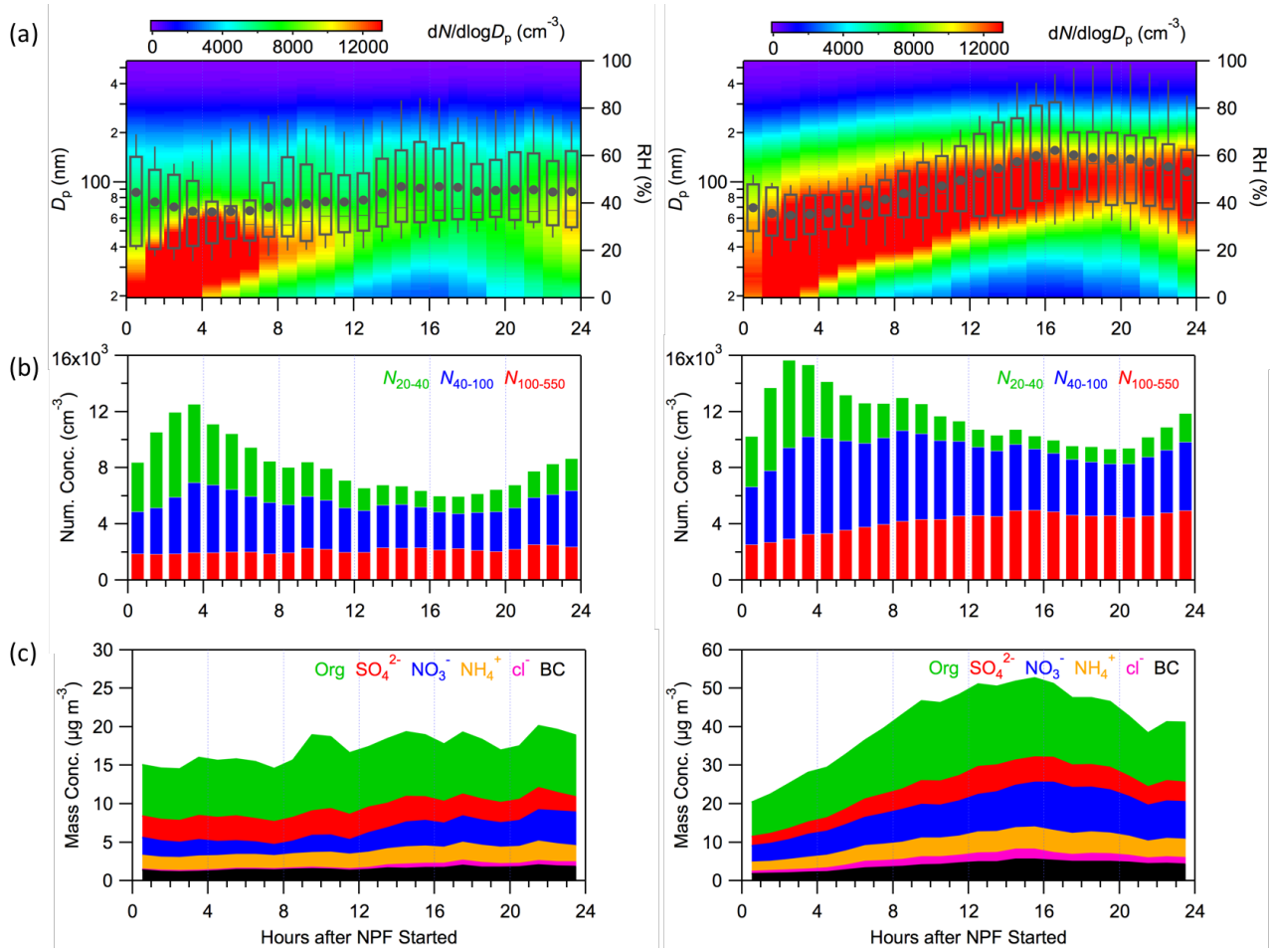

Supplementary Figure 6. Evolution of average (a) size-resolved particle number concentrations, and relative humidity (RH), (b) number concentrations of small Aitken mode ($N_{20\text{-}40}$), large Aitken mode ($N_{40\text{-}100}$), and accumulation mode ($N_{100\text{-}550}$) particles, (c) mass concentrations of submicron organics (Org), sulfate (SO_4^{2-}), nitrate (NO_3^-), ammonium (NH_4^+), chloride (cl^-), and black carbon (BC), after new particle formation started at 260 m. The left panels show the average evolution of 21 NPF events without continuous growth, whereas the right panels are the average evolution of 26 NPF events followed by clear particle growth. The gray box plots in (a) show the mean (diamonds), median (horizontal line), 25th and 75th percentiles (lower and upper box), and 10th and 90th percentiles (lower and upper whiskers) of RH.

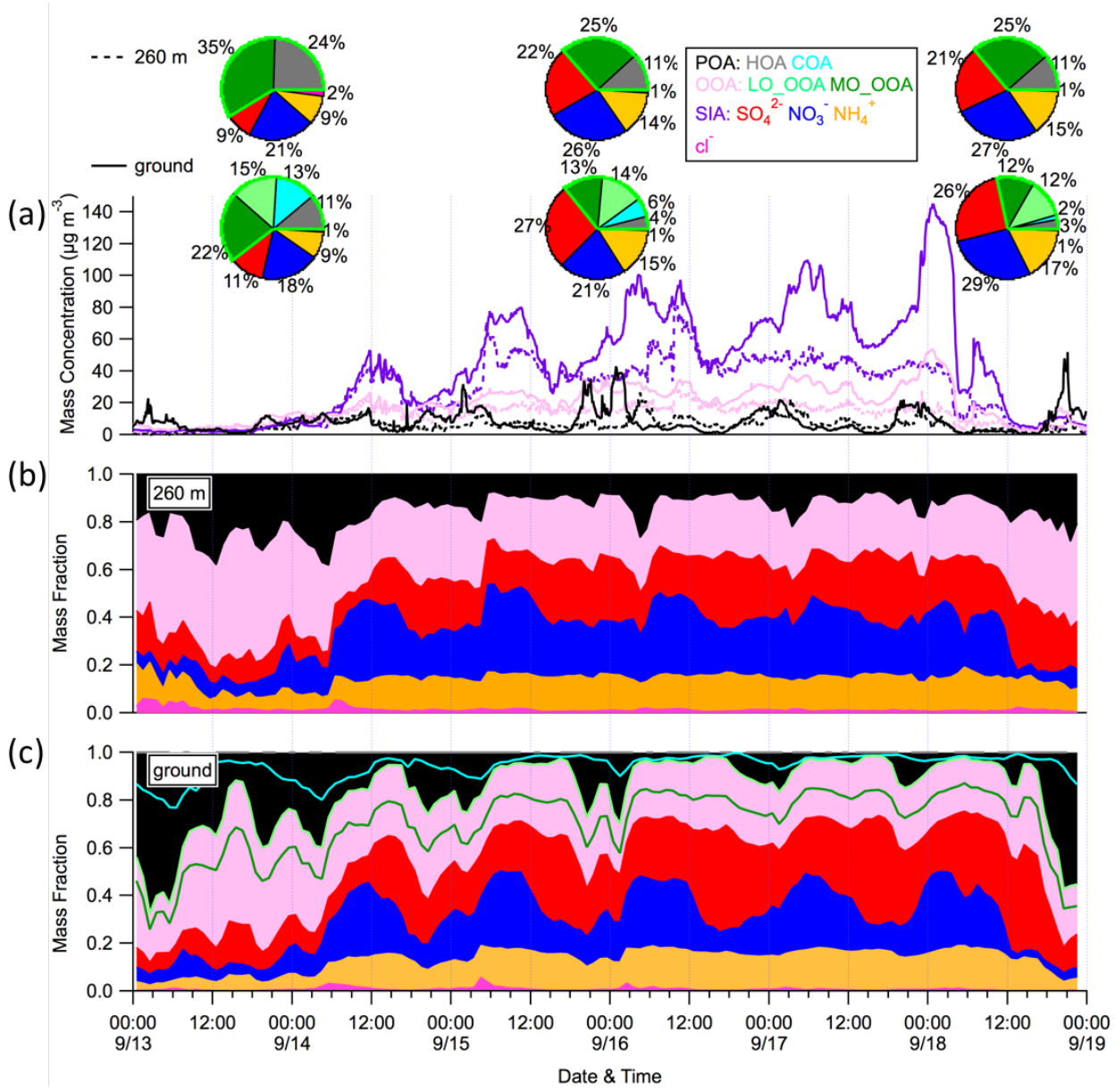

Supplementary Figure 7. (a) Time series of mass concentrations of primary organic aerosol (POA) including hydrocarbon-like OA (HOA) from traffic emissions and cooking-related OA (COA), secondary organic aerosol (SOA) including more oxidized oxygenated organic aerosol (MO-OOA) and less oxidized oxygenated organic aerosol (LO-OOA), secondary inorganic aerosol (SIA) including sulfate (SO_4^{2-}), nitrate (NO_3^-) and ammonium (NH_4^+), and chloride (cl^-) at ground level (solid lines) and 260 m (dash lines) during the severe pollution period of September 13 – 19, 2015. (b) and (c) shows the evolution of mass fractions of aerosol species at 260 m and ground level, respectively. The pie charts depict the average chemical composition during three periods, i.e., initiation, accumulation, and scavenge at 260 m (Top) and ground level (bottom), respectively.

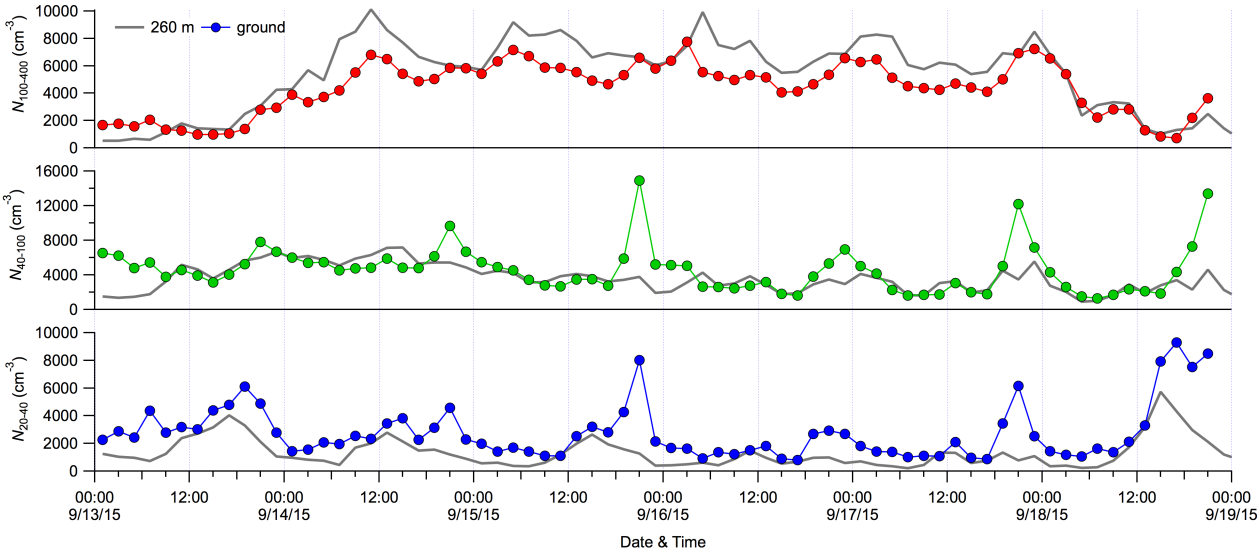

Supplementary Figure 8. Comparison of the number concentrations of three mode particles, i.e, small Aitken mode ($N_{20\text{-}40}$), large Aitken mode ($N_{40\text{-}100}$), and Accumulation mode ($N_{100\text{-}400}$) between ground level and 260 m from September 13 to 19, 2015.

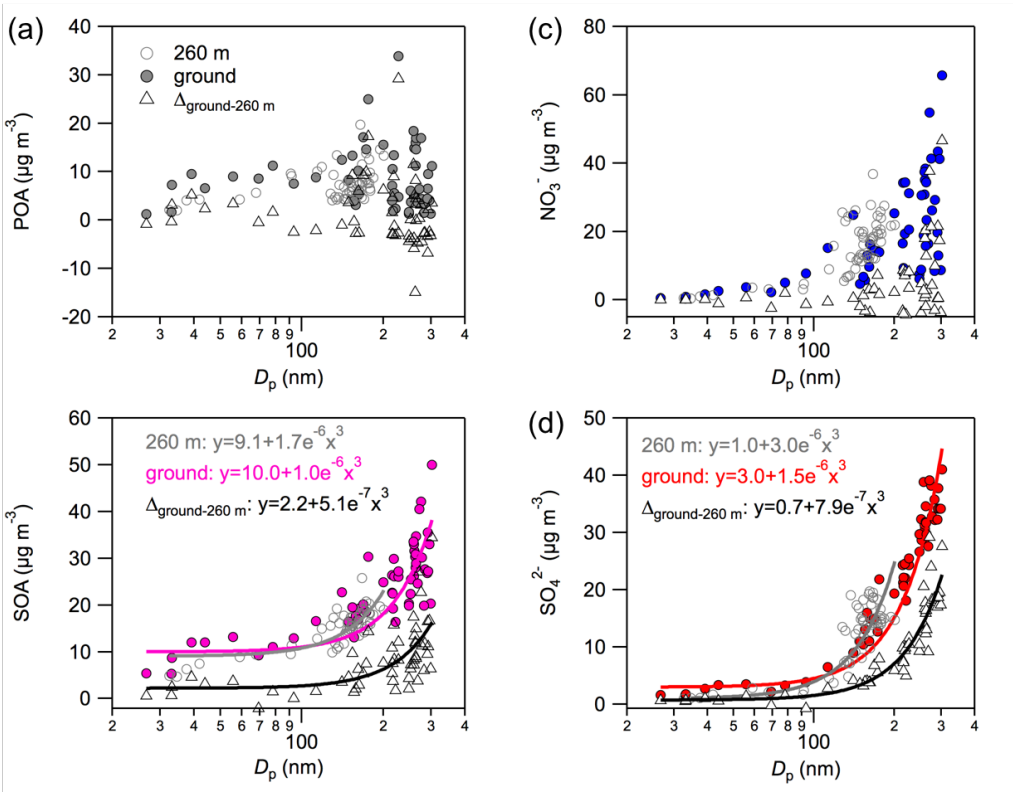

Supplementary Figure 9. Variations of mass concentrations of (a) primary organic aerosols (POA), (b) secondary organic aerosols (SOA), (c) nitrate (NO_3^-), (d) sulfate (SO_4^{2-}) as a function of geometric mean diameter (GMD) of new formed particles at 260 m (open circle) and ground level (solid circle) during the typical NPF event followed by a severe haze episode. The differences in mass concentrations of the two heights ($\Delta_{ground\text{-}260\ m}$) as a function of GMD of new formed particles at ground level (triangle) are also shown.

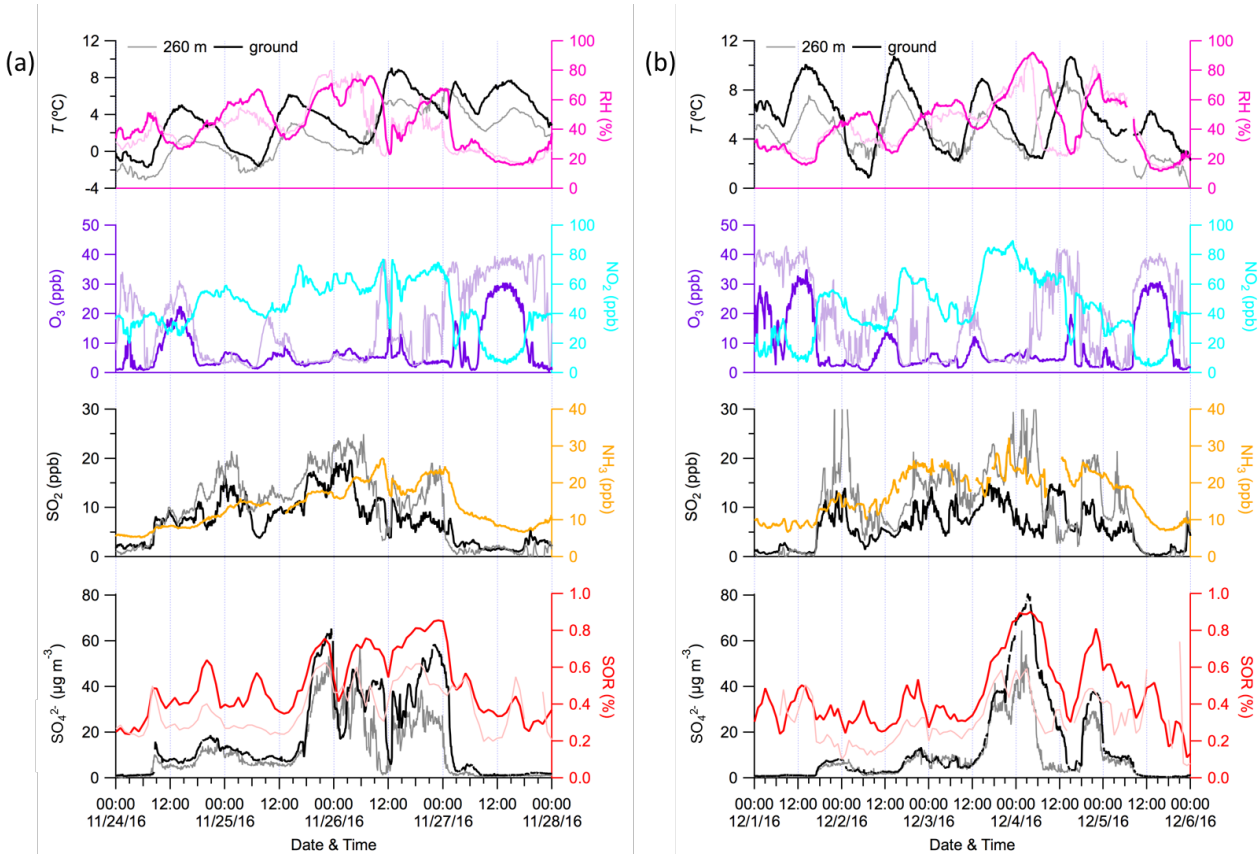

Supplementary Figure 10. The evolution of temperature (*T*), relative humidity (RH), ozone (O_3), nitrogen dioxide (NO_2), sulfur dioxide (SO_2), ammonia (NH_3), sulfate (SO_4^{2-}), and the molar fraction of sulfate in total sulfur (SOR) in two severe haze pollutions during (a) November 24 – 28, and (b) December 1 – 6, 2016.

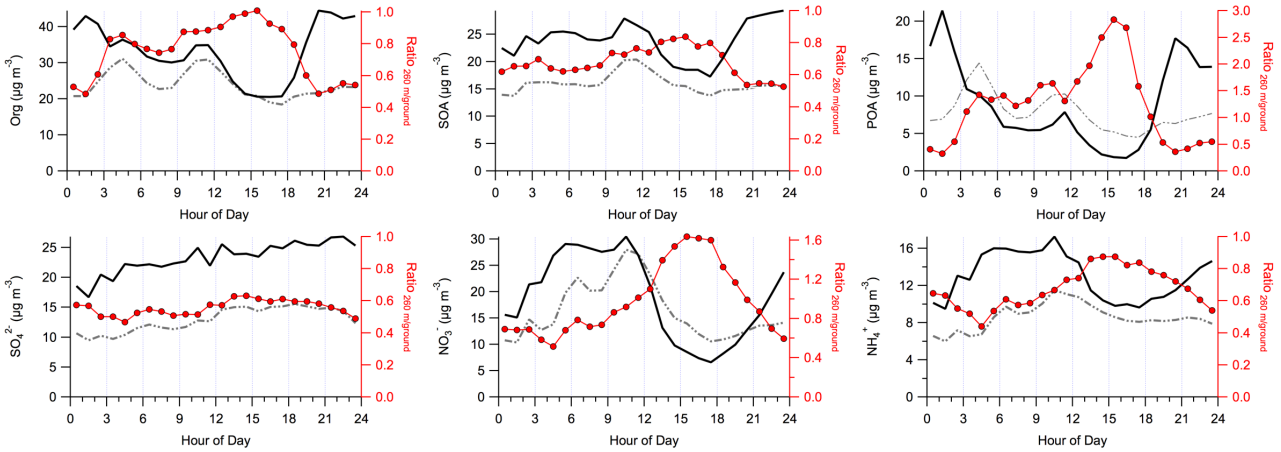

Supplementary Figure 11. Diurnal evolution of mass concentrations of organics (Org), secondary organic aerosol (SOA), primary organic aerosol (POA), sulfate (SO_4^{2-}), nitrate (NO_3^-), and ammonium (NH_4^+) at 260 m and ground level during the haze accumulation periods from September 14 to 18, 2015.

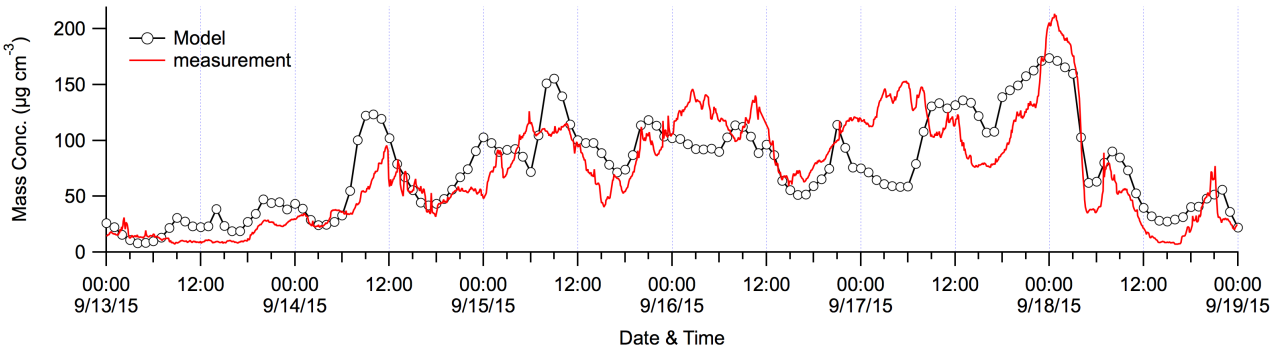

Supplementary Figure 12. Time series of simulated $PM_{2.5}$ and measured non-refractory submicron aerosols (NR-PM_1) concentration in urban Beijing.

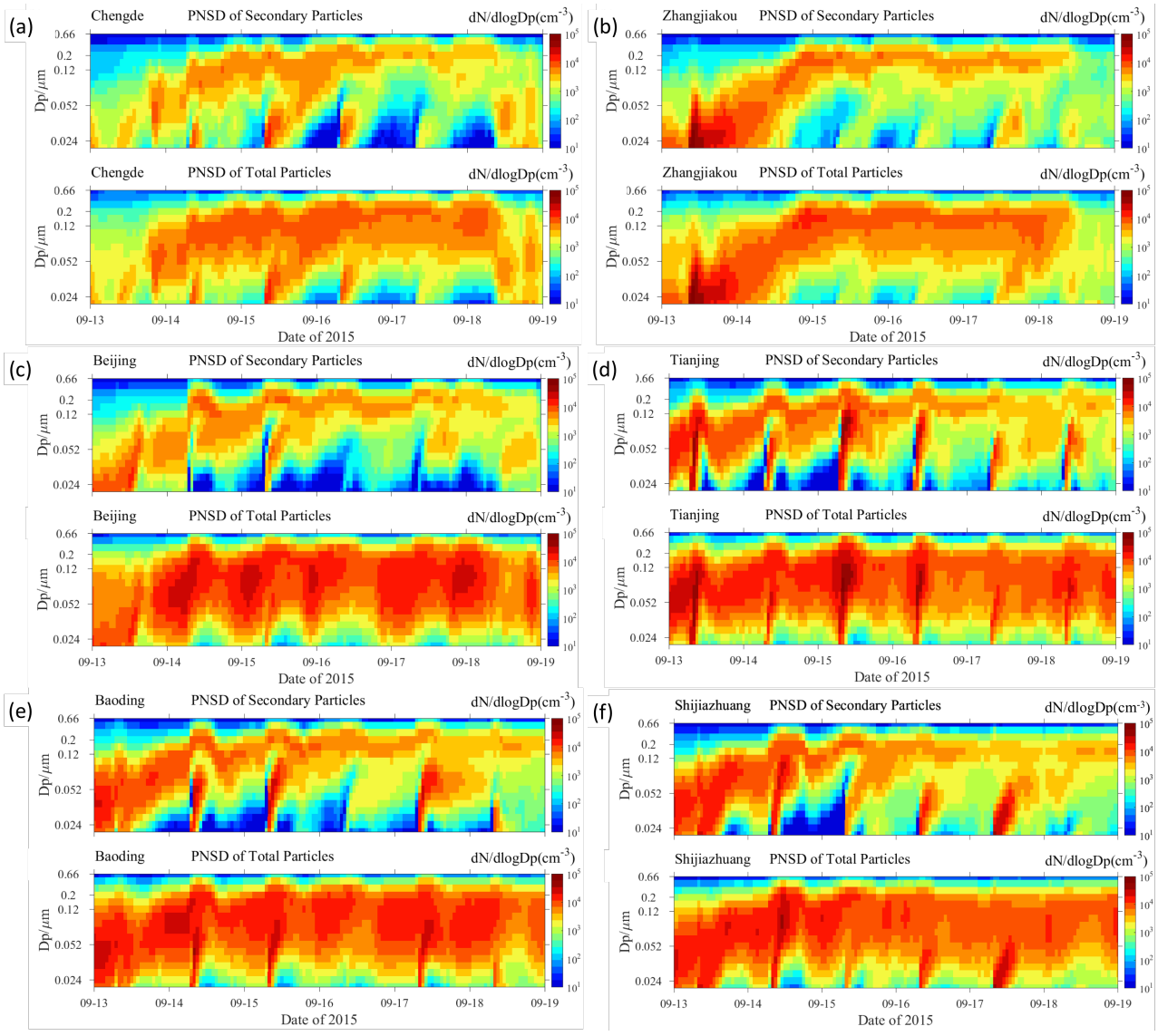

Supplementary Figure 13. The evolution of simulated particle number size distributions of new formed particles (PNSD of Secondary Particles), and total particles (PNSD of Total Particles) in (a) Chengde, (b) Zhangjiakou, (c) Beijing, (d) Tianjing, (e) Baoding, and (f) Shijiazhuang from September 13 to 19, 2015.

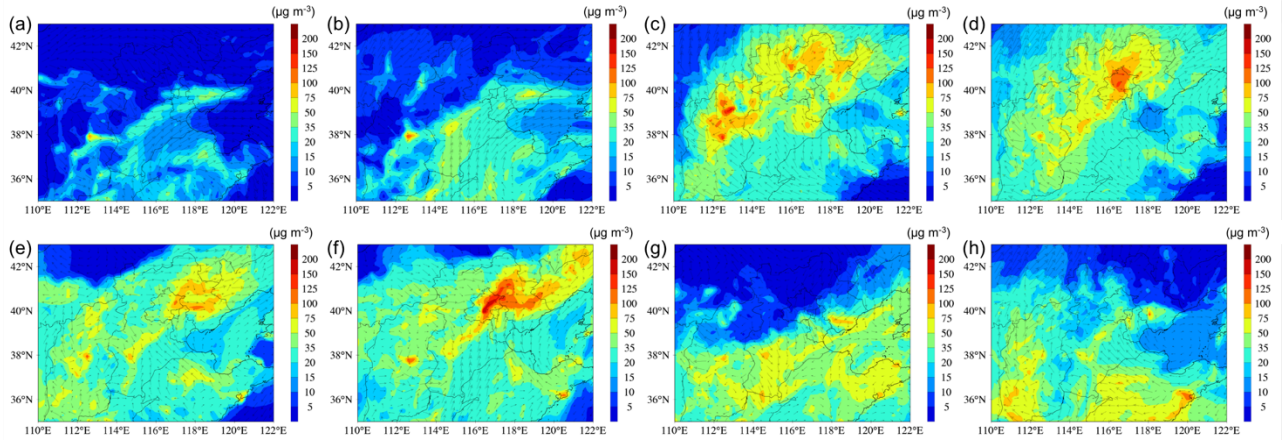

Supplementary Figure 14. (a) – (h) shows the evolution of spatial distribution of $PM_{2.5}$ from September 13 to 20, 2015 including Beijing-Tianjin-Hebei Area.

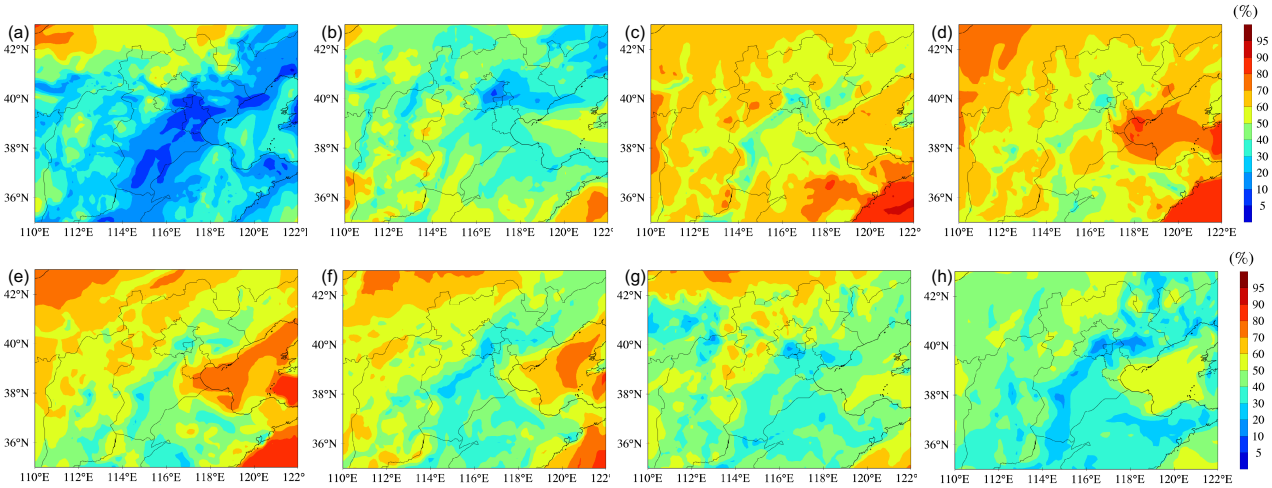

Supplementary Figure 15. (a) – (h) shows the evolution of spatial distribution of accumulation mode particle fractions that were contributed by the growth of new formed particles from September 13 to 20, 2015 in Beijing-Tianjin-Hebei Area.

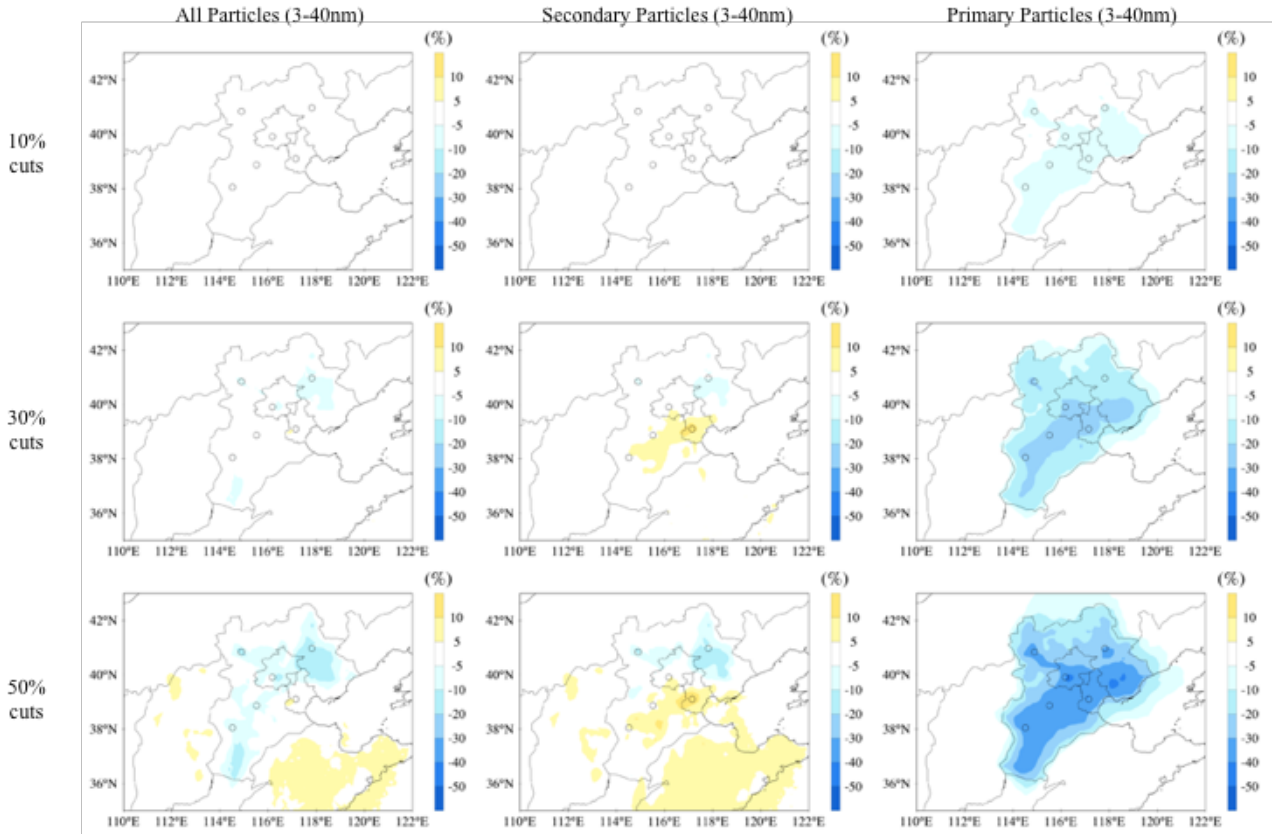

Supplementary Figure 16. The response of number concentration of all particles, secondary particles, and primary particles in the size range from 3 – 40 nm to emission cuts in the Beijing-Tianjin-Hebei Area in September, 2015. From the top to bottom, the emissions of both primary particles and gaseous precursors over Beijing-Tianjin-Hebei Area were cut by 10%, 30%, and 50%, respectively.

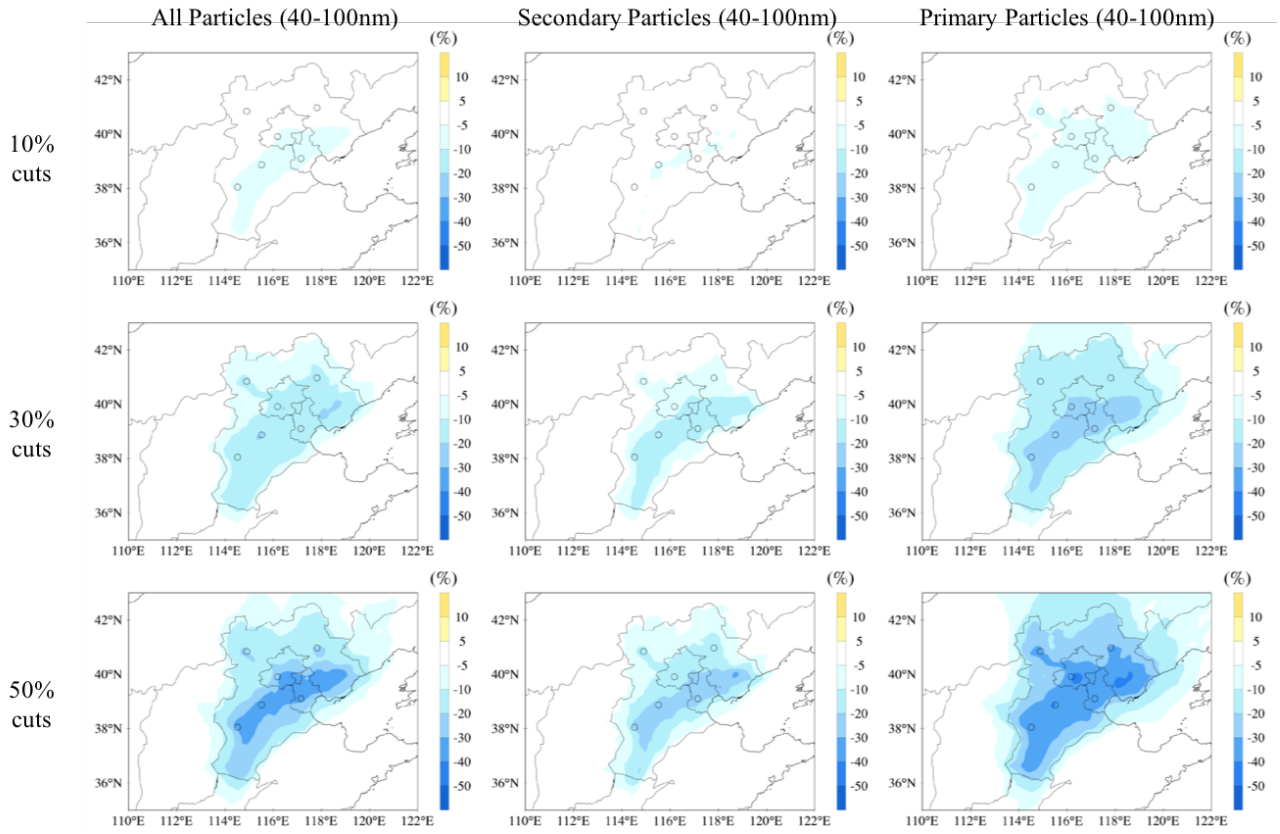

Supplementary Figure 17. The response of number concentration of all particles, secondary particles, and primary particles in the size range from 40 – 100 nm to emission cuts in the Beijing-Tianjin-Hebei Area in September, 2015. From the top to bottom, the emissions of both primary particles and gaseous precursors over Beijing-Tianjin-Hebei Area were cut by 10%, 30%, and 50%, respectively.

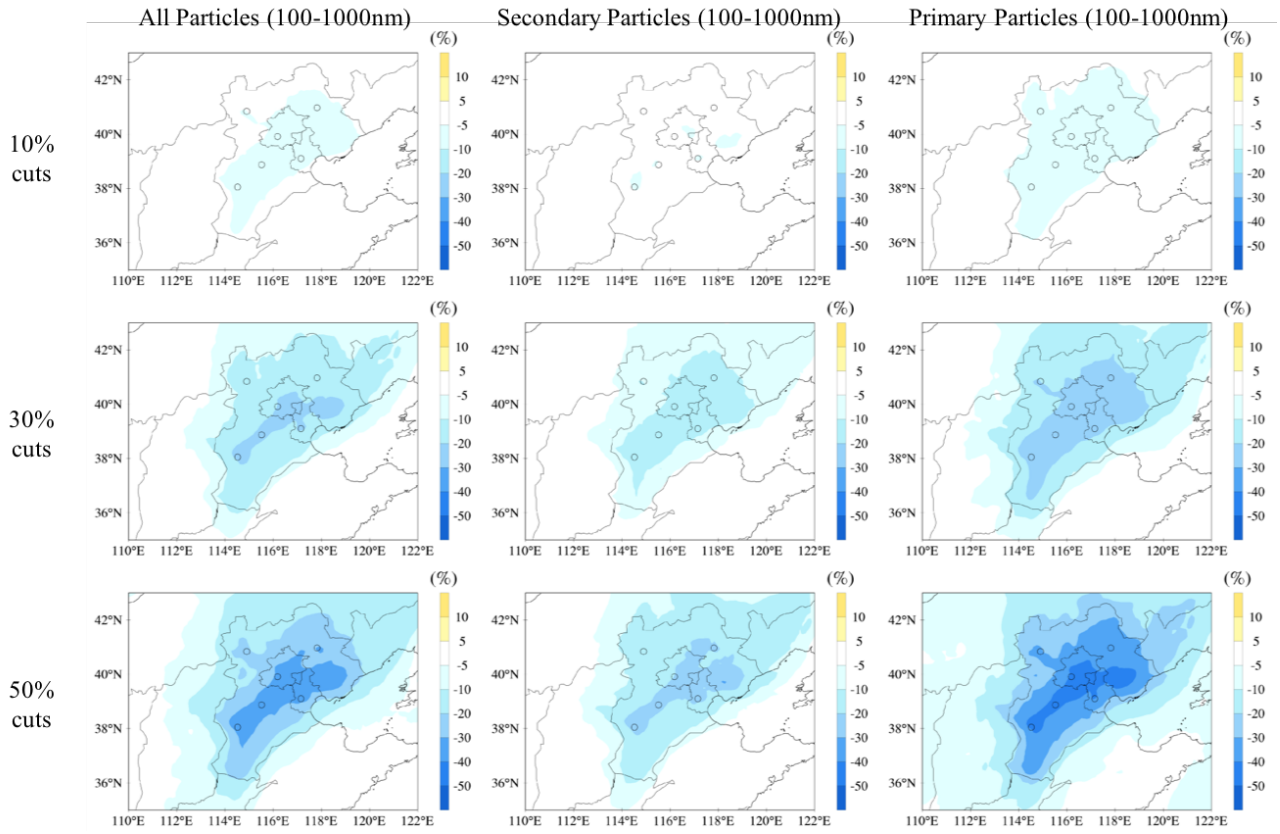

Supplementary Figure 18. The response of number concentration of all particles, secondary particles, and primary particles in the size range from 100 – 1000 nm to emission cuts in the Beijing-Tianjin-Hebei Area in September, 2015. From the top to bottom, the emissions of both primary particles and gaseous precursors over Beijing-Tianjin-Hebei Area were cut by 10%, 30%, and 50%, respectively.

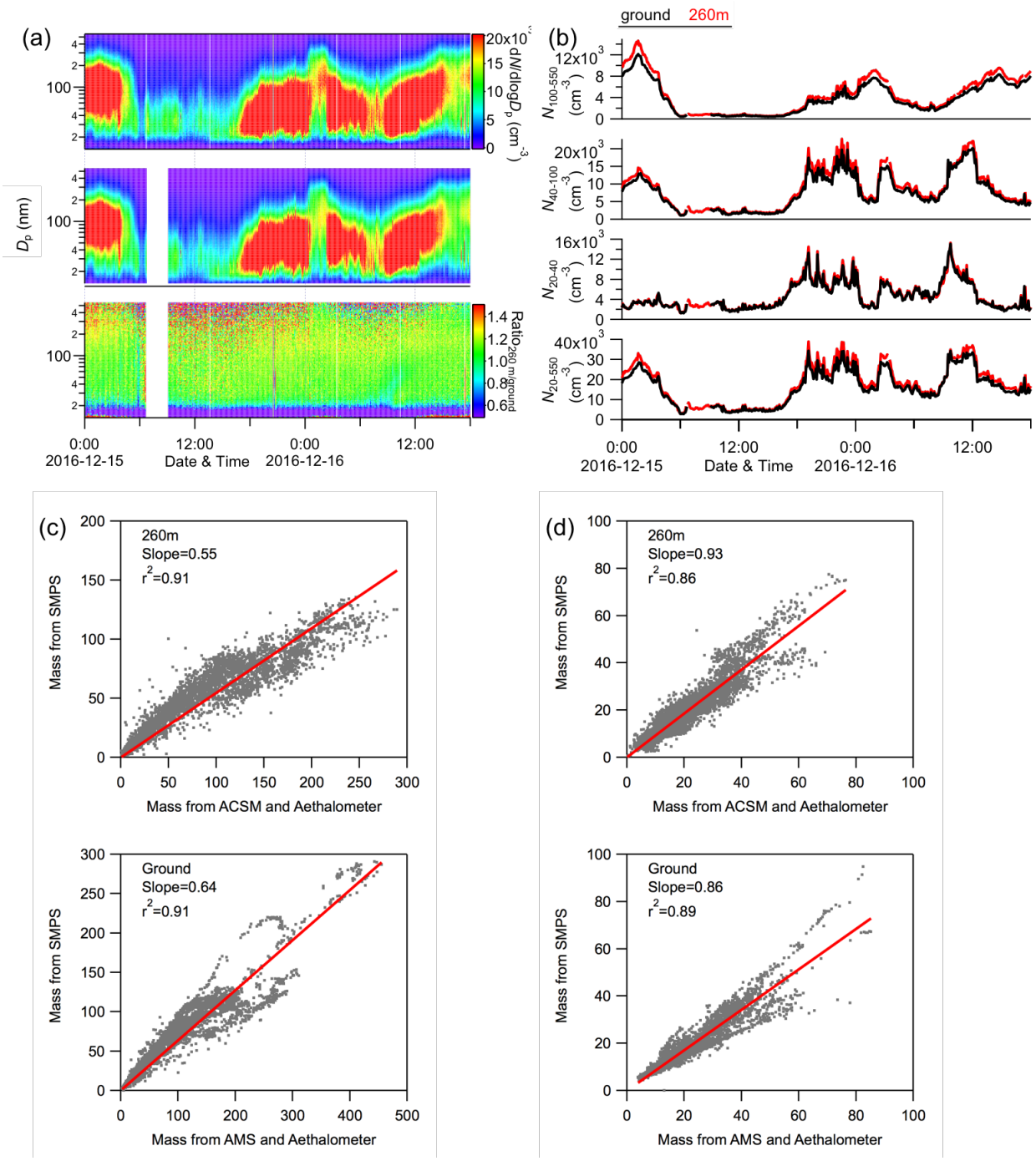

Supplementary Figure 19. An example of the inter-comparisons between two SMPSs: (a) particle number size distribution, (b) particle number concentration of different size mode. Scatter plots of the mass concentrations converted from the number concentrations of SMPS measurements versus PM_1 measured by HR-AMS/ACSM and AE at 260 m and ground level in (c) winter 2016 and (d) summer 2017.

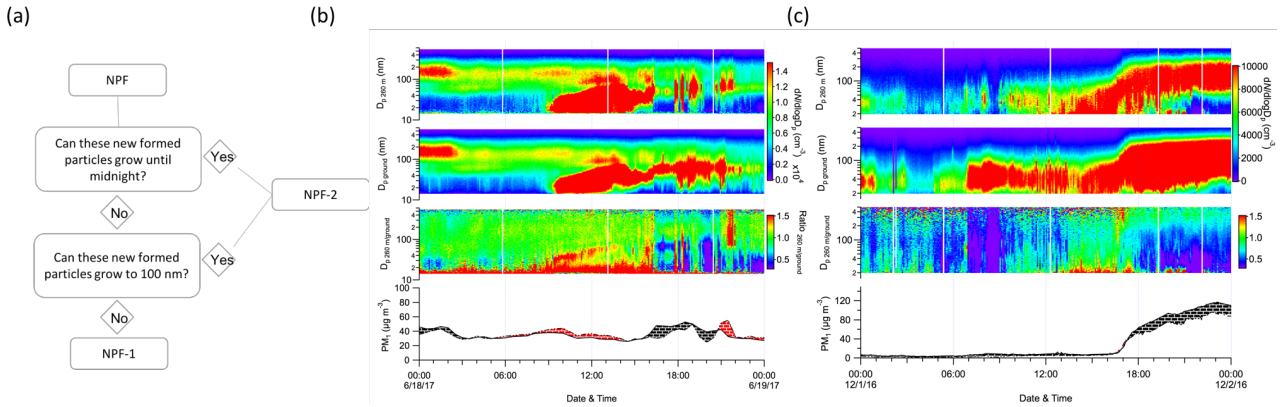

Supplementary Figure 20. (a) A flowchart of the decision path during the classification of the NPF events. (b) An example of the first type of new particle formation event (NPF-1). (c) An example of the second type of new particle formation event (NPF-2).

Supplementary Tables

Supplementary Table 1. An overview of three campaigns.

Date & Time	Season	PM_1 ($\mu g\ m^{-3}$)		NPF-1	NPF-2	Nighttime growth events
		260 m	ground			
08/22 – 10/01/2015	Fall	33.2	33.7	7	10	12
11/21 – 12/13/2016	Winter	64.7	83.4	5	6	4
06/01 – 06/26/2017	Summer	19.0	20.9	9	10	7

Supplementary Table 2. A summary of severe haze pollution events (PM_1 > 100 $\mu g\ m^{-3}$) during three campaigns. The formation and evolution of all these haze events were associated with an initiation of NPF in the beginning followed by continuous particle growth.

Date	Days	$PM_{1\ avg}$		$PM_{1\ max}$	
		260 m	ground	260 m	ground
13/09/2015	6	66.9	80.1	131.8	224.3
19/09/2015	4	59.4	70.8	104.5	185.7
23/09/2015	2	N/A*	63.2	N/A	124.3
23/11/2016	5	105.1	150.7	248.4	311.3
28/11/2016	3	68.1	95.7	155.1	195
01/12/2016	4	103.8	152.6	289.3	455.6
05/12/2016	4	69	94.2	162.2	196.4
09/12/2016	4	125.8	130.4	217	225.7

* data not available.

Supplementary Table 3. Night time growth events during three campaigns. The parameters including boundary layer (PBL), relative humidity (RH), temperature (*T*), condensation sink (CS), the initial particle size (Dp_0), growth rate (GR) and mass concentration of submicron aerosols (PM_1) during the growth period at 260 m (gray) and ground level (white).

Date	PBL (m)	RH (%)		*T* (°C)		CS (s^{-1})		GR (nm h^{-1})		PM_1 (μg m^{-3})	
26/08/15	180	52.4	57.3	25.4	26.5	0.02	0.01	0	5.7	N/A	18.0
02/09/15	376	49.5	52.5	26.2	27.1	0.02	0.02	2.2	3.1	11.5	17.1
03/09/15	550	79.9	71.0	23.7	25.7	0.03	0.04	9.2	12.8	37.1	44.7
07/09/15	643	59.0	54.3	22.5	24.3	0.04	0.05	4.4	4	33.4	37.2
08/09/15	609	59.1	58.3	22.3	24.0	0.06	0.07	0	6	61.3	65.4
14/09/15	433	52.7	59.3	20.1	21.1	0.06	0.06	2.3	3.4	44.5	67.2
15/09/15	1002	54.3	58.3	21.1	21.9	0.07	0.06	0	7	60.6	105.4
16/09/15	721	68.7	64.8	21.2	22.5	0.06	0.07	0	7.9	78.6	110.8
17/09/15	689	70.3	66.8	22.9	24.4	0.07	0.07	0	8	71.3	148.0
19/09/15	N/A*	54.7	48.1	22.6	24.3	0.05	0.04	0	5.5	28.1	44.0
20/09/15	N/A	59.8	60.0	21.7	22.8	0.04	0.05	6.5	6.8	N/A	52.7
23/09/15	385	75.0	68.8	21.0	22.6	0.04	0.04	0	4.9	27.5	45.9
24/11/16	344	42.8	47.7	0.4	2.1	0.08	0.11	0	9.4	99.4	128.9
27/11/16	368	29.0	36.8	1.6	2.5	0.04	0.05	22	22.6	30.2	35.4
28/11/16	236	32.9	45.6	3.8	3.9	0.05	0.12	0	12.1	38.3	83.1
01/06/17	501	40.8	36.6	21.0	23.7	0.02	0.03	4.8	4.2	15.1	11.1
03/06/17	284	38.9	38.3	21.0	22.8	0.03	0.03	4.1	N/A	17.6	N/A
07/06/17	234	40.3	40.2	25.6	27.0	0.04	0.05	4.4	5.7	18.5	24.6
08/06/17	186	25.7	31.0	27.3	27.7	0.02	0.04	0	3.6	5.6	20.1
13/06/17	209	56.4	58.0	22.1	23.8	0.03	0.04	0	4.5	19.9	N/A
14/06/17	473	20.6	20.8	30.8	32.4	0.02	0.03	0	4.8	10.5	N/A
25/06/17	N/A	55.9	62.7	24.4	25.3	0.01	0.04	0	3.8	N/A	20.1

* N/A means no data or growth did not observed.

Supplementary References

1 Wiedensohler, A. *et al.* Mobility particle size spectrometers: harmonization of technical standards and data structure to facilitate high quality long-term observations of atmospheric particle number size distributions. *Atmos. Meas. Tech.* **5**, 657-685, doi:10.5194/amt-5-657-2012 (2012).

2 Zhao, J. *et al.* Insights into aerosol chemistry during the 2015 China Victory Day parade: results from simultaneous measurements at ground level and 260 m in Beijing. *Atmos. Chem. Phys.* **17**, 3215-3232, doi:10.5194/acp-17-3215-2017 (2017).

3 Jayne, J. T. *et al.* Development of an Aerosol Mass Spectrometer for Size and Composition Analysis of Submicron Particles. *Aerosol Sci. Tech.* **33**, 49-70, doi:10.1080/027868200410840 (2000).

4 Middlebrook, A. M., Bahreini, R., Jimenez, J. L. & Canagaratna, M. R. Evaluation of Composition-Dependent Collection Efficiencies for the Aerodyne Aerosol Mass Spectrometer using Field Data. *Aerosol Sci. Tech.* **46**, 258-271, doi:10.1080/02786826.2011.620041 (2012).

5 Sun, Y. *et al.* Real-Time Characterization of Aerosol Particle Composition above the Urban Canopy in Beijing: Insights into the Interactions between the Atmospheric Boundary Layer and Aerosol Chemistry. *Environ. Sci. Technol.* **49**, 11340-11347, doi:10.1021/acs.est.5b02373 (2015).

6 Tang, G. *et al.* Mixing layer height and its implications for air pollution over Beijing, China. *Atmos. Chem. Phys.* **16**, 2459-2475, doi:10.5194/acp-16-2459-2016 (2016).

7 DeCarlo, P. F., Slowik, J. G., Worsnop, D. R., Davidovits, P. & Jimenez, J. L. Particle Morphology and Density Characterization by Combined Mobility and Aerodynamic Diameter Measurements. Part 1: Theory. *Aerosol Sci. Tech.* **38**, 1185-1205, doi:10.1080/027868290903907 (2004).